Enhanced thermoelectric performance of n-type filled skutterudite In$_x$Co$_4$Sb$_{12}$

Feng Gao[1,2], Ying Lei[1,2,3,4,*], Xiaowu Jiang[2,5], Yu Li[2,*] , Jin Qiu[2], Chao Yong[2], Xingxiang Fan[4], and Rundong Wan[6]

[1] The State Key Laboratory of Vanadium and Titanium Resources Comprehensive Utilization, Pangang Group Research Institute Co., Ltd., Panzhihua 617000, China

[2] School of Metallurgical Engineering, Anhui University of Technology, Ma'anshan 243032, China

[3] College of Materials and Metallurgy, Guizhou University, Guiyang 550025, China

[4] School of Chemistry and Resources Engineering, Honghe University, Mengzi 661199, China

[5] Ironmaking Plant of Shanghai Meishan Iron and Steel Limited by Share Co., Ltd., Nanking 210039, China

[6] College of Materials Science and Engineering, Kunming University of Science and Technology, Kunming 650093, China

ABSTRACT

In-single-filled In$_x$Co$_4$Sb$_{12}$ skutterudite was synthesized from high-purity raw materials by microwave heating for 5 min, and the bulk materials with 7.26–7.64 g cm^{-3} density are subsequently achieved after annealing and spark plasma sintering. The XRD detected results show that all major diffraction peaks are indexed to the body-centered cubic CoSb$_3$ and InSb secondary phase which are found to be present in all samples. Pores and dislocations are observed in In$_x$Co$_4$Sb$_{12}$, while those microstructure characteristics may reduce the lattice thermal conductivity by scattering different frequency phonons. Indium atoms optimize the carrier concentration and InSb may act as an n-type dopant to provide impurity carriers and increase the mobility. The optimal carrier concentration is obtained as 4.77×10^{20} cm^{-3} in In$_{0.6}$Co$_4$Sb$_{12}$. The maximum power factors of 3720 μWm^{-1} K^{-2} are observed from In$_{0.4}$Co$_4$Sb$_{12}$. The lattice thermal conductivity of In$_{0.6}$Co$_4$Sb$_{12}$ was effectively reduced to 1.12 Wm^{-1} K^{-1}. The highest *ZT* of 1.15 appears at 773 K and possible larger values can be achieved at a higher temperature.

Feng Gao and Ying Lei have equally contributed to this work.

Address correspondence to E-mail: leiyingahut@163.com; liyuahut@163.com

Ⓓ Springer

1 Introduction

Thermoelectric conversion technology is one of the feasible option which can convert waste heat into electrical energy directly, free of secondary pollution. The application of thermoelectric conversion technology depends on the material performances which are determined by the figure of merit (ZT), which is defined as $ZT = \sigma S^2 \, T/\kappa$, where σ, S, T, k are the electrical conductivity, Seebeck coefficient, temperature, and thermal conductivity, respectively. Thus, high-performance thermoelectric materials require optimized electrical and thermal transport properties synchronously, that is, a combination of large S, appropriate σ, and lowest possible k [1].

Skutterudites have a general formula of XY_3, where X and Y are transition metals (Co, Ir, Rh, etc.) and phosphorus group elements (P, As, Sb, etc.). They have body-centered cubic structure with space group of I$m3$ as well as 8 XY_3 units and 32 atoms in each unit cell [2]. The pristine $CoSb_3$ has a high lattice thermal conductivity of $\sim 10 \, Wm^{-1} \, K^{-1}$ on account of strong covalent bond between CO and Sb. For many thermoelectric materials, such as Bi_2Te_3 [3], Mg_3Sb_2 [4], and Si [5], composite materials are mostly used to reduce the lattice thermal conductivity [6, 7], but these processes are complicated and lengthy. Thanks to the crystal structure of $CoSb_3$, a simple method can be used to reduce its lattice thermal conductivity. Filling impurity atoms into the lattice voids in $CoSb_3$ allows one to strongly reduce the thermal conductivity on account of phonon-resonant scattering and synchronously optimize the carrier concentration. The filler atoms that have been reported in literatures include alkali metal elements [8, 9], alkali earth metal elements [10], rare earth elements [11–14], and others [10, 15, 16]. Hitherto, the thermoelectric transport properties of indium single-filled $CoSb_3$ have been reported in many literatures [16–19]. Despite the success of these studies, since the performance of materials is closely related to the preparation methods, it is still necessary to discuss the thermoelectric transport mechanism if a new fabrication method was adopted.

The filled skutterudites are usually achieved via melting [10, 14, 19], high-pressure synthesis [9, 13], solid-state reaction [11, 20], or hydrothermal synthesis [21]. Microwave is a high-efficiency and energy-saving heating way which has been widely used in the synthesis of inorganic materials [22]. In addition to this work, there is only one paper related to the microwave synthesis of filled skutterudites [23]. In this work, series of In-single-filled $In_xCo_4Sb_{12}$ bulks are fabricated via microwave ultrafast synthesis combined with spark plasma sintering. The phase composition and microstructure are discussed in detail. The variations of carrier concentration, mobility, conductivity, Seebeck coefficient, thermal conductivity, and lattice thermal conductivity are discussed in detail. Our desire is to provide a feasible approach for the efficient preparation of high-performance thermoelectric materials.

2 Experimental section

2.1 Sample synthesis

In-single-filled skutterudite samples $In_xCo_4Sb_{12}$ were synthesized by a combination of microwave synthesis and high-temperature annealing. The stoichiometric quantities were weighed according to the nominal compositions of $In_xCo_4Sb_{12}$ (x = 0.3, 0.4, 0.6, 0.8, 0.10, 0.12). The fabrication procedures are as follows: (1) The mixture powders were fully ground and then cold-pressed as $\sim$ 15 mm buttons, (2) the as-pressed button was vacuum sealed in a fused silica tube and then put into corundum crucible in a microwave oven, using copper oxide powder as microwave receptors, (3) the synthesis reaction was conducted with a microwave power of 1100 W for 5 min, (4) the as-synthesized ingot was subsequently annealed under vacuum at 948 K for 5 days, (5) the as-annealed ingot was ground into powder and sintered on SPS for 10 min at the temperature of 923 K and pressure of 50 MPa, and (6) the as-sintered bulk was cut into pieces on low-speed diamond saw and then applied to various characterizations.

2.2 Structural characterization and thermoelectric transport properties

Powder X-ray diffraction (PXRD) data were collected on D8-ADVANCE diffractometer with CuKα radiation to check the phase composition. The morphologies and elemental distributions were observed on Nano-SEM430 field-emission scanning electron microscopy (FE-SEM) and X-ray energy-dispersive spectroscopy (EDS), respectively. The

microstructures were observed on Talos F200S high-angle annular dark-field scanning transmission electron microscopy (STEM). Bright-field and high-angle annular dark-field (HAADF) STEM images were photographed to get information of the atomic arrangement. The room-temperature Hall coefficient and carrier concentration were measured on Resi-test 8300 Hall effect tester. The electrical transport properties were measured by the standard four-probe method on Joule Yacht/Namicro-3 test system from room temperature to 773 K. Thermal diffusion coefficients were measured on LFA-427 laser thermal conducting instrument from room temperature to 773 K and the total thermal conductivity κ was subsequently determined according to $\kappa = C_p D d$, where C_p, D, d are heat capacity (0.23 $J \cdot g^{-1} \cdot K^{-1}$ [20]), thermal diffusion coefficient, and density. The electronic thermal conductivity κ_{el} was determined according to $\kappa_{el} = LT\sigma$, where L, T, σ are Lorenz number ($2.0 \times 10^{-8} V^2 K^{-2}$ [19]), temperature, and conductivity. Finally, the lattice thermal conductivity was obtained as κ_{lat} as $\kappa_{lat} = \kappa - \kappa_{el}$.

3 Results and discussion

3.1 Structural characterization

Figure 1a shows the powder XRD patterns of In_x-Co_4Sb_{12} after SPS, and all major diffraction peaks are indexed to the body-centered cubic $CoSb_3$ phase (Im3, JCPDS#89-4871). In comparison with the samples synthesized via traditional melting and solid-state reaction, the synthesis time is shortened from hours or a dozen hours to 5 min [16, 18]. Figure 1b shows the magnified XRD patterns of $In_xCo_4Sb_{12}$ between 23° and 40°, and InSb is found in all samples. InSb and other eutectic impurity phases, i.e., $CoSb_2$, Co, and Sb are clearly observed in the samples with the nominal indium fraction x higher than 0.80, indicating that the eutectic reaction in In–Sb–Co system seems to be unavoidable [16]. The diffraction peak intensity of eutectic impurity phases increases with the increased indium fraction, suggesting that there is a solubility limit of indium in $CoSb_3$ which is generally considered as 0.22–0.27 according to different reports [24]. As shown in Table 1, the lattice constants of 9.053–9.058 angstrom for $In_xCo_4Sb_{12}$ calculated by Jade6 are very close to that of the In-single-filled skutterudites achieved via different methods [16, 25].

As given in Table 1, the densities of $In_xCo_4Sb_{12}$ with increasing indium fractions are 7.26, 7.41, 7.42, 7.38, and 7.64 g/cm^3, respectively, measured by Archimedes' drainage method, which are close to the theoretical density of pristine $CoSb_3$ of 7.64 g/cm^3 [26]. The relative density of the sample reaches about 94%, and the good densities effectively enhance the charge transport which affects the electrical properties. Figure 2a and b shows the FESEM images of the

Fig. 1 a Powder XRD patterns of $In_xCo_4Sb_{12}$ and b magnified PXRD patterns between 23° and 40°
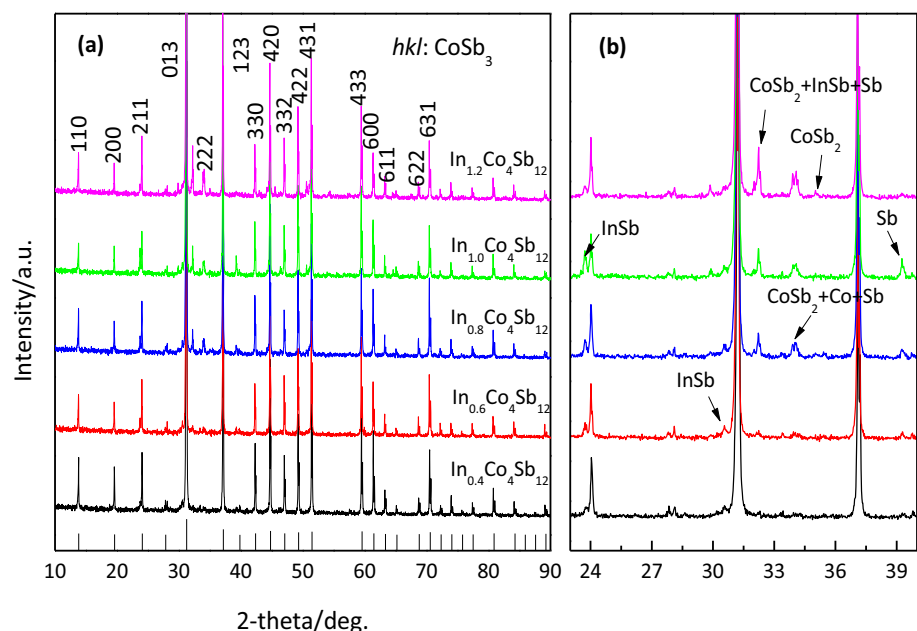
**Table 1** Related physical properties of $In_xCo_4Sb_{12}$ at room temperature

Nominal composition	a (Å)	ρ (g/cm^3)	d (%)	n (cm^{-3})	μ_H (cm^2/Vs)	m^* (m$_e$)
CoSb$_3$ [22]	9.0347	7.51		5.14×10^{17}	69.8	0.025
In$_{0.4}$Co$_4$Sb$_{12}$	9.0528	7.26	96.29	1.86×10^{20}	14.1	2.77
In$_{0.6}$Co$_4$Sb$_{12}$	9.0569	7.41	96.96	4.77×10^{20}	3.5	4.59
In$_{0.8}$Co$_4$Sb$_{12}$	9.0551	7.42	95.80	2.33×10^{20}	4.5	2.63
In$_{1.0}$Co$_4$Sb$_{12}$	9.0577	7.38	94.03	1.73×10^{20}	7.4	2.00
In$_{1.2}$Co$_4$Sb$_{12}$	9.0581	7.64	96.09	1.68×10^{20}	9.7	1.92
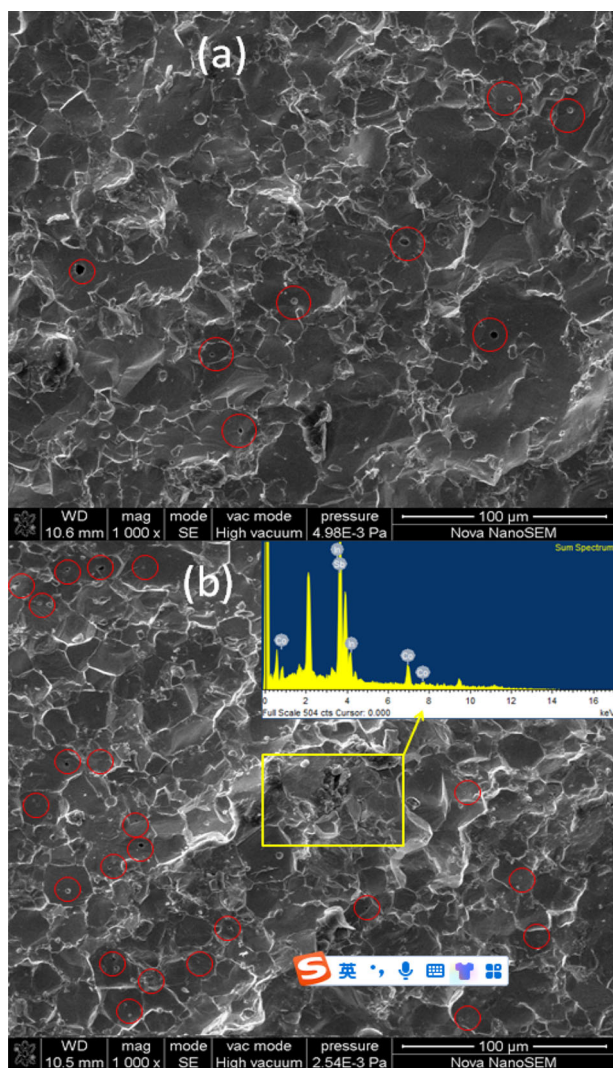
Fig. 2 Field emission SEM (FESEM) image of the cross sections of **a** In$_{0.4}$Co$_4$Sb$_{12}$ and **b** In$_{0.6}$Co$_4$Sb$_{12}$, and the EDX spectra of an area of a rectangular with height–width of 48.5 × 69.7 μm in In$_{0.6}$Co$_4$Sb$_{12}$ (inset)

cross sections of In$_{0.4}$Co$_4$Sb$_{12}$ and In$_{0.6}$Co$_4$Sb$_{12}$, respectively. The average grain size of In$_{0.4}$Co$_4$Sb$_{12}$ and In$_{0.6}$Co$_4$Sb$_{12}$ were measured as 15.9 and 16.8 μm (Nano Measurer/Fudan University), while the grain

size and numbers of grain boundaries are close to each other. As marked by red circles in Fig. 2a and b, a large number of micron and submicron pores were found in the matrix grains, which may be attributed to the evaporation of residual trace air. The inset image in Fig. 2b shows the EDX spectra of an area of a rectangular with height–width of 48.5 × 69.7 μm in In$_{0.6}$Co$_4$Sb$_{12}$. The EDX result reveals that the molar ratios of In, Co, and Sb are 4.22%, 22.4%, and 73.38%, respectively, suggesting the presence of InSb in the selected region consistent with the PXRD detection result in Fig. 1b.

The microstructures of In$_{0.6}$Co$_4$Sb$_{12}$ are further examined. Figure 3b shows the BFSTEM image of In$_{0.6}$Co$_4$Sb$_{12}$, and it shows relatively complete CoSb$_3$ host grains and clear grain boundaries. Figure 3a and c shows the HRSTEM images of the selected red frame regions in Fig. 3b, respectively. Figure 3a displays the inner lattice fringes inside CoSb$_3$ grain, and it shows no obvious dislocation. The insets show the fast Fourier transform (FFT) image and atomic arrangement of the selected red box regions, respectively. Figure 3b displays the HRSTEM image of grain boundary, and the FFT and inverse fast Fourier transform (IFFT) images acquired from the selected square red wireframe region. Significant screw dislocations are found on grain boundary, and the dislocation lines are basically parallel to the slip direction indicated by the red arrow. Figure 3e shows the BFSTEM image of In$_{0.6}$Co$_4$Sb$_{12}$ and it shows high-concentration dislocations and remarkable distortions. The corresponding HRSTEM images for the selected red frame regions are shown in Fig. 3d and f, respectively. The IFFT images clearly show the details of edge dislocations inside CoSb$_3$ grain. The eutectic reaction results in the uneven distribution of impurity atoms in CoSb$_3$ host grains, and the ultra-high heating rate introduced by microwave and subsequent air quenching provides a condition for the generation of supersaturated vacancy [27], as a
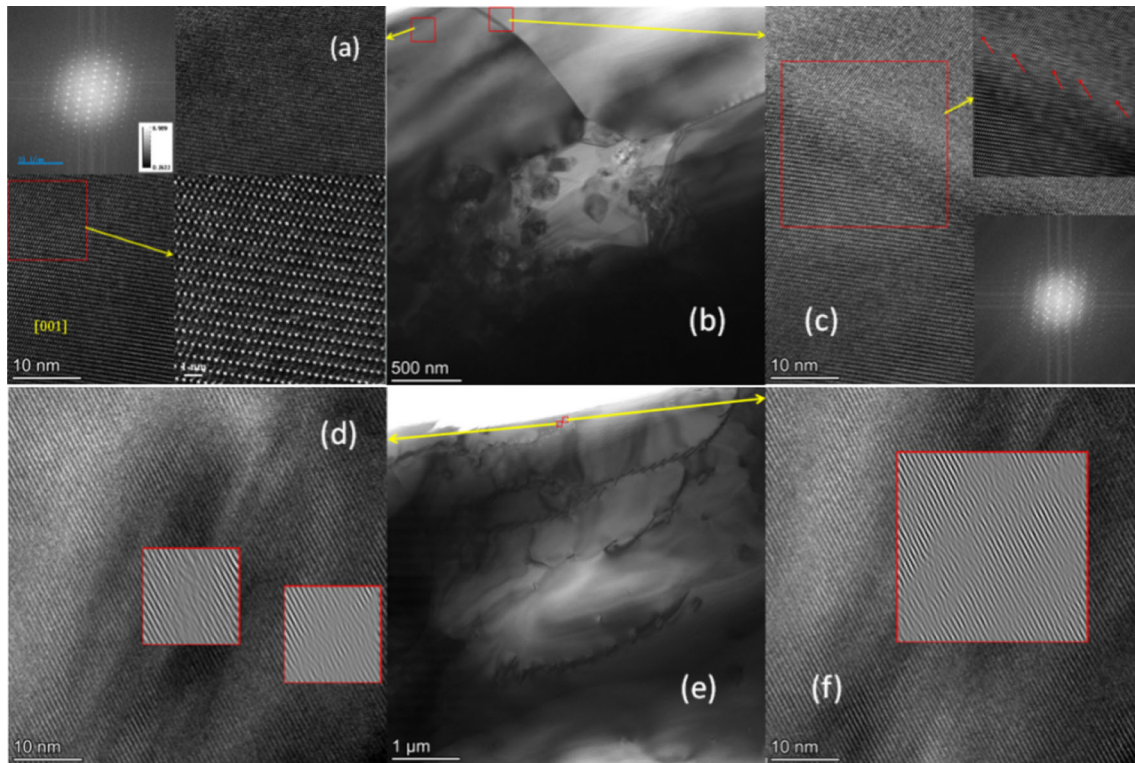
Fig. 3 **a** HRSTEM image of $CoSb_3$ host grain, the top left inset and bottom right inset, respectively, show the FFT and enlarge image in red box region; **b** BFSTEM image of $CoSb_3$ host grain and grain boundary in $In_{0.6}Co_4Sb_{12}$; **c** HRSTEM image of $CoSb_3$ grain boundary, the upper right and bottom right insets, respectively, show the inverse FFT and FFT images in red box region; **d** HRSTEM image of $CoSb_3$ host grain, the insets, respectively, show the inverse FFT images in red box region; **e** BFSTEM image of $CoSb_3$ host grains and dislocations in $In_{0.6}Co_4Sb_{12}$; **f** HRSTEM image of $CoSb_3$ host grain, the inset shows the inverse FFT image in red box region

result to promote the formation of dislocations. High-concentration dislocations can effectively scatter medium wavelength phonons and further decrease the lattice thermal conductivity, and this enhancement mechanism has been confirmed and applied in the optimization design of variety of thermoelectric materials [1, 11, 28].

3.2 Thermoelectric transport performances

The variations of room-temperature carrier concentration and mobility with indium nominal fraction are shown in Table 1 and Fig. 4a. The carrier concentrations of binary $CoSb_3$ and $In_xCo_4Sb_{12}$ are 5.14×10^{17} and $1.68 \times 10^{20} \sim 4.77 \times 10^{20}$ cm^3, respectively, which are increased by two or three orders of magnitude after filling treatment. Although indium atoms in filled skutterudites can be regarded as ionic impurities, the carrier still experiences the transport dominated by electron–phonon scattering, indicating that indium filling can increase carrier

concentration by enhancing electron–phonon scattering. This mechanism is not affected by the type of filler, but they can provide different number of carriers to achieve the optimal electric transport performance of the whole system. That is the reason why the carrier concentrations observed in the present samples are close to those of other single-filled or multi-filled skutterudites [11, 14, 19, 20]. The carrier concentration in $In_xCo_4Sb_{12}$ first increases and then decreases with the increasing indium fractions, which is similar to literature reports [12]. The possible reason is that samples with different filling fractions have different effects on the lattice potential field, which is related to the effective mass due to various phase compositions. As shown in Table 1, the effective masses m^* of the samples with $x = 0.4$, 0.6, 0.8, 1.0, and 1.2 are, respectively, calculated as 2.77, 4.59, 2.63, 2.00, and 1.92 m_e (m_e is the bare electron mass) according to the single parabolic band (SPB) model. Apparently, the variation trend of carrier
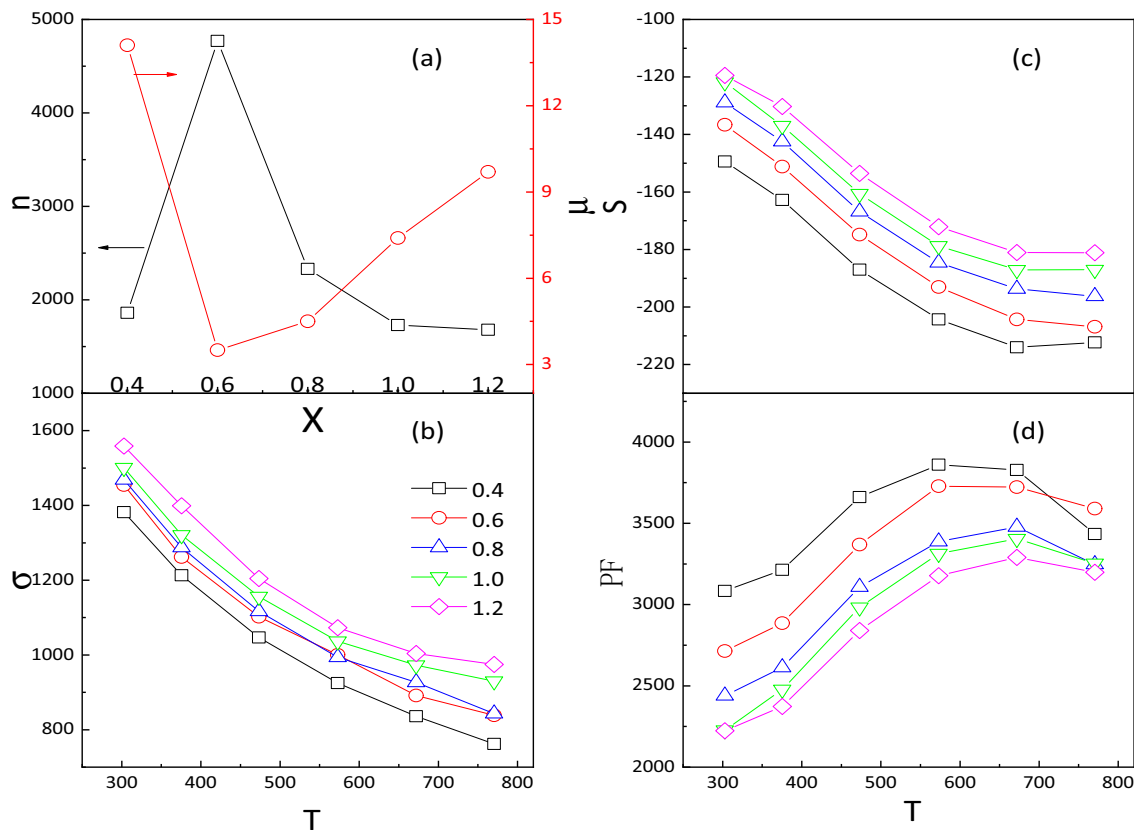
Fig. 4 Electrical transport properties for $In_xCo_4Sb_{12}$: **a** conductivity, **b** Seebeck coefficient, **c** variations of room-temperature carrier concentration and mobility with indium nominal fraction, and **d** power factor

concentration is completely consistent with that of effective mass. The carrier concentration of 4.77×10^{20} in $In_{0.6}Co_4Sb_{12}$ is close to the optimum carrier of 5.0×10^{20} for filled skutterudites [11, 14]. The mobility increases with the increase of the filling fraction when the indium content $x \geq 0.4$. It has been reported that the carrier mobility of InSb is as high as 10^4 cm^2/Vs [29], hence the increase of mobility may be related to the increase of InSb secondary phase content of larger indium fraction. Since the carrier mobility is negatively correlated with the effective mass, the variation trend of carrier mobility is just opposite to the variation trend of effective mass.

Figure 4b shows the temperature dependence of electrical conductivity of $In_xCo_4Sb_{12}$ between room temperature and 773 K. The electrical conductivity decreases with temperature thus exhibiting a semi-metallic or degenerate semiconducting behavior. The room-temperature electrical conductivity of $In_xCo_4Sb_{12}$ in the order of indium fraction is, respectively, 224, 236, 238, 243, and 253 times larger than that of the pristine CoSb$_3$ [27]. The variation of room-

temperature electrical conductivity in the order of indium fraction is exactly consistent with the product of carrier concentration and mobility list in Table 1. Similar to the literature reports [16–18, 21], as indium fraction increases, the electrical conductivity increases, indicating that InSb phase in $In_xCo_4Sb_{12}$ acts as an n-type dopant to provide more impurity carriers and increase the mobility.

Figure 4c shows the temperature dependence of Seebeck coefficient of $In_xCo_4Sb_{12}$ between room temperature and 773 K. The absolute values of the Seebeck coefficient of n-type $In_xCo_4Sb_{12}$ increase with temperature exhibiting a semi-metallic or degenerate semiconducting behavior. The variation trends of Seebeck coefficient with indium fraction are just opposite to those of electrical conductivity. The Seebeck coefficient is also proportional to the effective mass and inversely proportional to the two-thirds power of carrier concentration. The maximum values of the Seebeck coefficients are -214.0, -206.9, -196.2, -187.1, -181.1 μVK^{-1} in the order of filling fractions, respectively.

The comprehensive electrical properties are determined by power factor which is defined as $PF = S\sigma^2$. The temperature dependence of the power factors of $In_xCo_4Sb_{12}$ is shown in Fig. 4d. The power factors increase with indium fraction, and they increase initially from room temperature to about 673 K and then decrease between 673 and 773 K. The maximum power factors of 3861 and 3729 $\mu Wm^{-1} K^{-2}$ are observed from $In_{0.4}Co_4Sb_{12}$ and $In_{0.6}Co_4Sb_{12}$, respectively.

Figure 5a shows the total thermal conductivity of $In_xCo_4Sb_{12}$ as a function of temperature between 300 and 773 K. The room-temperature thermal conductivity is significantly reduced in comparison with that of the pristine $CoSb_3$. The room-temperature thermal conductivity of $CoSb_3$ is 9.22 $Wm^{-1} K^{-1}$, while it is, respectively, lowered to 3.35, 3.33, 4.12, 4.39, and 4.90 $Wm^{-1} K^{-1}$ in the order of filling fractions. Over the entire test temperature range, the thermal conductivity basically decreases with filling fractions. Furthermore, the thermal conductivity of all the samples decreases with increasing temperature from room temperature to 673 K, and increases slightly with increasing temperature from 673 to 773 K. The minimum thermal conductivity of all the samples, respectively, are 2.61, 2.42, 2.94, 3.25, and 3.47 $Wm^{-1} K^{-1}$ in the order of filling fractions. The upper right inset displays the variations of electron thermal conductivity for all samples, as it shows that the electron thermal conductivity strictly increases with the increased filling fractions and its contribution to the total thermal conductivity increases gradually.

Figure 5b shows the lattice thermal conductivity of $In_xCo_4Sb_{12}$ as a function of temperature between 300 and 773 K, and its variation trend is consistent with that of total thermal conductivity. Apparently, the variation trend of the lattice thermal conductivity in $In_xCo_4Sb_{12}$ is very similar to that of the total thermal conductivity, and it makes a major contribution to the total thermal conductivity within the investigated temperature range. The minimum values of lattice thermal conductivity, respectively, are 1.48, 1.12, 1.69, 1.86, and 2.02 $Wm^{-1} K^{-1}$ in the order of filling fractions. As shown in Fig. 2, much more sintering pores were found in $In_{0.6}Co_4Sb_{12}$ than those of $In_{0.4}Co_4Sb_{12}$, which results in further reduction of lattice thermal conductivity via scattering more low-frequency phonons [17]. The lowest lattice thermal conductivity of 1.12 $Wm^{-1} K^{-1}$ in $In_{0.6}Co_4Sb_{12}$ in the present study is remarkably low as compared with that of similar compositions which are fabricated using different procedures [16, 30, 31].

Figure 6a shows the temperature dependence of thermoelectric figure of merits (ZT). The ZT for the In-filled $In_xCo_4Sb_{12}$ increases with temperature. $In_{0.6}Co_4Sb_{12}$ shows the maximum ZT of 1.15 at 773 K. It is noted that larger values may be achieved at a higher temperature. The highest ZT in this work is larger than those of In-single-filled skutterudite samples produced by other techniques [17, 21, 31], and it is very close to that of the state-of-the-art samples reported in literatures [16, 24]. Figure 6b shows the Seebeck coefficients, PF and ZT for all concentrations of samples at 773 K. $In_{0.6}CoSb_3$ sample obtained moderate Seebeck coefficient and the highest PF and ZT values. This work provides a promising technique for the manufacturing of high-performance thermoelectric bulks. Moreover, the thermoelectric transport performances still have potential for further optimization.
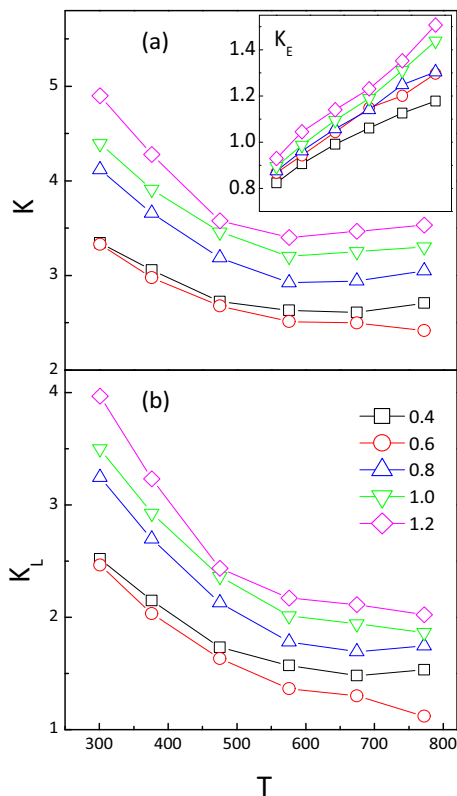
Fig. 5 Thermal transport properties for $In_xCo_4Sb_{12}$: **a** thermal conductivity, **b** lattice thermal conductivity
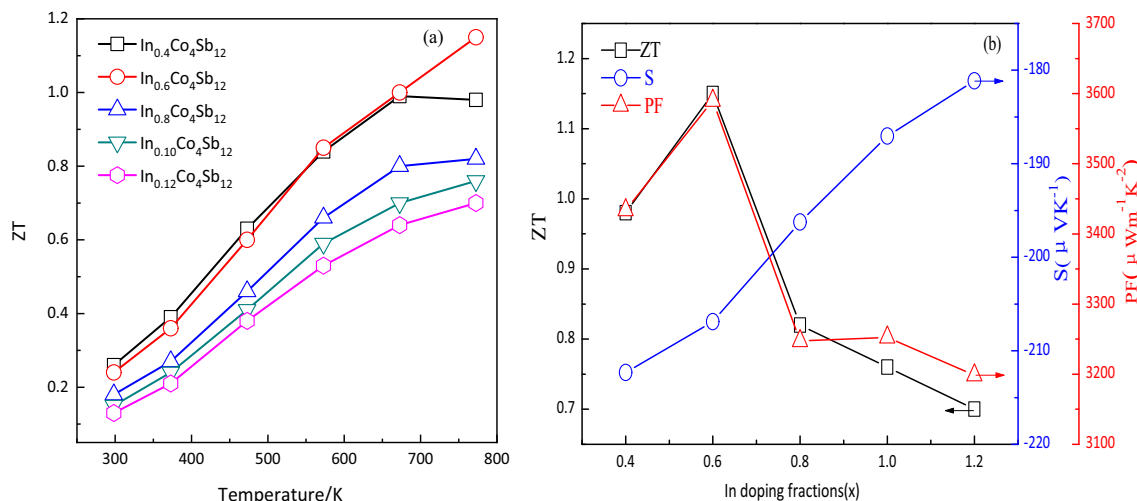
Fig. 6 a Thermoelectric figure of merits (ZT) of $In_xCo_4Sb_{12}$, **b** Seebeck coefficients, PF and ZT for all concentrations of samples at 773 K

4   Conclusion

In summary, a new technology to fabricate In-single-filled n-type $In_xCo_4Sb_{12}$ skutterudites thermoelectric bulks via Microwave synthesis combined with SPS sintering is described. Skutterudites phase was obtained in 5-min microwave heating time. InSb second phase is found in all samples and the solubility limit of indium is around 0.2–0.3 for $CoSb_3$. Indium atoms optimize the carrier concentration by resonance scattering, and InSb phase may act as an n-type dopant to provide more impurity carriers and increase the mobility. The maximum power factors of 3861 and 3729 $\mu Wm^{-1}\,K^{-2}$ are observed from $In_{0.4}Co_4Sb_{12}$ and $In_{0.6}Co_4Sb_{12}$, respectively. $In_{0.6}Co_4Sb_{12}$ shows the highest ZT of 1.15 at 773 K and possible larger values can be achieved at a higher temperature. Future work, such as the multiple filling of indium in combination with other elements, is expected to further improving the comprehensive electrical properties and reduce the lattice thermal conductivity synchronously.

Author contributions

FG: investigation, resources, writing—original draft; YL: conceptualization, methodology, funding acquisition, supervision, resources, writing—original draft, writing—review & editing; XJ: investigation, formal analysis, validation, resources; YL: conceptualization, methodology, funding acquisition, supervision, project administration, writing—review & editing; JQ: formal analysis and resources; CY: resources; XF: resources; RW: writing—review & editing.

Funding

Data availability

Data will be made available on reasonable request.

Declarations

Competing interests There are no conflicts to declare.

References

1. J. Yang, H. Yip, A. Jen, Rational design of advanced thermoelectric materials. Adv. Energy Mater. **3**, 549–565 (2013)

2. C. Hu, X. Zeng, Y. Liu, M. Zhou, H. Zhao, T.M. Tritt, J. He, J. Jakowski, P.R.C. Kent, J. Huang, B.G. Sumpter, Effects of partial La filling and Sb vacancy defects on $CoSb_3$ skutterudites. Phys. Rev. B. **95**, 165204 (2017)

3. M.S. Shalaby, H.M. Hashem, N.M. Yousif, H.A. Zayed, A. Sotelo, L.A. Wahab, Preparation, structural characteristics and optical parameters of the synthesized nano-crystalline sulphur-doped $Bi_2Te_{2.85}Se_{0.15}$ thermoelectric materials. J. Mater. Sci. Mater. Electron **31**, 10612–10627 (2020)

4. Y. Lin, M. Wood, K. Imasat, J.J. Kuo, D. Lam, A.N. Mortazavi, T.J. Slade, S.A. Hodge, K.X.M.G. Kanatzidis, D.R. Clarke, M.C. Hersam, G.J. Snyder, Expression of interfacial Seebeck coefficient through grain boundary engineering with multi-layer graphene nanoplatelets. Energy Environ. Sci. **13**, 4114–4121 (2020)

5. Y. Li, G. Wang, M. Akbari-Saatlu, M. Procek, H.H. Radamson, Si and SiGe nanowire for micro-thermoelectric generator: a review of the current state of the art. Front Mater. **77**, 045202 (2021)

6. M.S. Shalaby, S. Abdelhaleem, A. Sotelo, $(Bi_2Te_3)_{1-x}(PANI)_x$ compositions-synthesis, structural, spectroscopic characterization with enhanced thermoelectric performance. Synthetic Met. **285**, 117025 (2022)

7. A.E. Shalan, A.S.H. Makhlouf, S. Lanceros-Mendez, Advances in nanocomposite materials for environmental and energy harvesting applications. Eng. Mat. **959**, 1 (2022)

8. Z.G. Mei, J. Yang, Y.Z. Pei, W. Zhang, L.D. Chen, J. Yang, Alkali-metal-filled $CoSb_3$ skutterudites as thermoelectric materials: theoretical study. Phys. Rev. B **77**, 045202 (2008)

9. J. Gainza, F. Serrano-Sánchez, J.E. Rodrigues, J. Prado-Gonjal, N.M. Nemes, N. Biskup, O.J. Dura, J.L. Martínez, F. Fauth, J.A. Alonso, Unveiling the correlation between the crystalline structure of M-Filled $CoSb_3$(M=Y, K, Sr) skutterudites and their thermoelectric transport properties. Adv. Funct. Mater. **30**, 2001651 (2020)

10. W. Zhao, P. Wei, Q. Zhang, H. Peng, W. Zhu, D. Tang, J. Yu, H. Zhou, Z. Liu, X. Mu, D. He, J. Li, C. Wang, X. Tang, J. Yang, Multi-localization transport behaviour in bulk thermoelectric materials. Nat. Commun. **6**, 6197 (2015)

11. X. Meng, Z. Liu, B. Cui, D. Qin, H. Geng, W. Cai, L. Fu, J. He, Z. Ren, J. Sui, Grain boundary engineering for achieving high thermoelectric performance in n-Type skutterudites. Adv. Energy Mater. **7**, 1602582 (2017)

12. Y. Tang, R. Hanus, S. Chen, G.J. Snyder, Solubility design leading to high figure of merit in low-cost Ce-$CoSb_3$ skutterudites. Nat. Commun. **6**, 7584 (2015)

13. F. Serrano-Sánchez, J. Prado-Gonjal, N.M. Nemes, N. Biskup, M. Varela, O.J. Dura, J.L. Martínez, M.T. Fernández-Díaz, F. Fauth, J.A. Alonso, Low thermal conductivity in La-filled cobalt antimonide skutterudites with an inhomogeneous filling factor prepared under high-pressure conditions. J. Mater. Chem. A **6**, 118–126 (2018)

14. W. Li, J. Wang, Y. Xie, J.L. Gray, J.J. Heremans, H.B. Kang, B. Poudel, S.T. Huxtable, S. Priya, Enhanced thermoelectric performance of Yb-single-filled skutterudite by ultralow thermal conductivity. Chem. Mater. **1**, 862–872 (2019)

15. R.P. Hermann, R.Y. Jin, W. Schweika, F. Grandjean, D. Mandrus, B.C. Sales, G.J. Long, Einstein oscillators in thallium filled antimony skutterudites. Phys. Rev. Lett. **90**, 505 (2003)

16. Y.L. Tang, Y.T. Qiu, L.L. Xi, X. Shi, W.Q. Zhang, L.D. Chen, S.M. Tseng, S.W. Chen, G.J. Snyder, Phase diagram of In–Co–Sb system and thermoelectric properties of In-Containing skutterudites. Energy Environ. Sci. **7**, 812–819 (2014)

17. N. Gostkowska-Lekner, B. Trawinski, A. Kosonowski, B. Bochentyn, M. Lapinski, T. Miruszewski, K. Wojciechowski, B. Kusz, New synthesis route of highly porous $In_xCo_4Sb_{12}$ with strongly reduced thermal conductivity. J. Mater. Sci. **55**, 13658–13674 (2020)

18. V.V. Khovaylo, T.A. Korolkov, A.I. Voronin, M.V. Gorshenkov, A.T. Burkov, Rapid preparation of $In_xCo_4Sb_{12}$ with a record-breaking ZT = 1.5: the role of the in overfilling fraction limit and Sb overstoichiometry. J. Mater. Chem. A **5**, 3541–3546 (2017)

19. X. Shi, J. Yang, J.R. Salvador, M. Chi, J.Y. Cho, H. Wang, S. Bai, J. Yang, W. Zhang, L. Chen, Multiple-filled skutterudites: high thermoelectric figure of merit through separately optimizing electrical and thermal transports. J. Am. Chem. Soc. **133**, 7837–7846 (2011)

20. W.Y. Zhao, P. Wei, Q.J. Zhang, C.L. Dong, L.S. Liu, X.F. Tang, Enhanced thermoelectric performance in barium and indium double-filled skutterudite bulk materials via orbital hybridization induced by indium filler. J. Am. Chem. Soc. **131**, 3713–3720 (2009)

21. A. Gharleghi, P.C. Hung, F.H. Lin, C.J. Liu, Nanocomposites fabricated by hydrothermal synthesis combined with solid–vapor reaction: a signature of phonon-glass and electron-crystal materials. ACS Appl. Mater. Interfaces **8**, 35123–35131 (2016)

22. H.J. Kitchen, S.R. Vallance, J.L. Kennedy, N. Ruiz, L. Carassiti, A. Harrison, A.G. Whittaker, T.D. Drysdale, S.W. Kingman, D.H. Gregory, Modern microwave methods in solid-state inorganic materials chemistry: from fundamentals to manufacturing. Chem. Rev. **114**, 1170–1206 (2014)

23. K. Biswas, S. Muir, M. Subramanian, Rapid microwave synthesis of indium filled skutterudites: an energy efficient

route to high performance thermoelectric materials. Mater. Res. Bull. **46**, 2288–2290 (2011)

24. T. He, J. Chen, H.D. Rosenfeld, M.A. Subramanian, Thermoelectric properties of indium-filled skutterudites. Chem. Mater. **18**, 759–762 (2006)

25. M. Benyahia, V. Ohorodniichuk, E. Leroy, A. Dauscher, B. Lenoir, E. Alleno, High thermoelectric figure of merit in mesostructured $In_{0.25}Co_4Sb_{12}$ n-type skutterudite. J. Alloys Compd. **735**, 1096–1104 (2018)

26. A. Mochel, I. Sergueev, N. Nguyen, G.J. Long, F. Grandjean, D.C. Ohnson, R.P. Hermann, Lattice dynamics in the $FeSb_3$ skutterudite. Phys. Rev. B **84**, 64302–64309 (2011)

27. Y. Lei, W.S. Gao, R. Zheng, Y. Li, W. Chen, L.B. Zhang, R.D. Wan, H.W. Zhou, Z.Y. Liu, P.K. Chu, Ultrafast synthesis of Te-doped $CoSb_3$ with excellent thermoelectric properties. ACS Appl. Energy Mater. **2**, 4477–4485 (2019)

28. L. You, Y.F. Liu, X. Li, P.F. Nan, B.H. Ge, Y. Jiang, P.F. Luo, S.S. Pan, Y.Z. Pei, W.Q. Zhang, G.J. Snyder, J. Yang, J.Y. Zhang, J. Luo, Boosting the thermoelectric performance of PbSe through dynamic doping and hierarchical phonon scattering. Energy Environ. Sci. **11**, 1848–1858 (2018)

29. Q.S. Zhang, Z. Xiong, J. Jiang, W. Li, G.J. Xu, S.Q. Bai, P. Cui, L.D. Chen, Enhanced thermoelectric performance in $In_{1-x}Ga_xSb$ originating from the scattering of point defects and nanoinclusion. J. Mater. Chem. **21**, 12398–12401 (2011)

30. J. Eilertsen, S. Rouvimov, M.A. Subramanian, Rattler-seeded InSb nanoinclusions from metastable indium-filled $In_{0.1}Co_4Sb_{12}$ skutterudites for high-performance thermoelectrics. Acta Materialia. **60**, 2178–2185 (2012)

31. G.H. Li, K. Kurosaki, Y. Ohishi, H. Muta, S. Yamanaka, Thermoelectric properties of indium-added skutterudites $In_xCo_4Sb_{12}$. J. Electron. Mater. **42**, 1463–1468 (2013)